Photodissociation of HN_3 at 248 nm and Longer Wavelength: A CASSCF Study

Wei-Hai Fang†

Department of Chemistry, Beijing Normal University, Beijing 100875, People's Republic of China

Received: September 21, 1999; In Final Form: December 3, 1999

In the present work, photodissociation of HN_3 at 248 nm and longer wavelength is investigated with the complete active space SCF (CASSCF) molecular orbital method. The stationary points on the ground- and excited-state potential energy surfaces are fully optimized at the CASSCF level with cc-pVDZ and cc-pVTZ basis sets. The potential energy profiles, governing HN_3 dissociation to NH + N_2 and H + N_3, are characterized with the multireference MP2 (CASPT2) algorithm. The pathways leading to different products are determined on the basis of the obtained potential energy surfaces of dissociation and their crossing points. A comparison is made among the present and previous theoretical results and experimental findings. The present study provides an insight into the mechanism of the UV photodissociation of HN_3 at a wavelength range from 355 to 248 nm.

Introduction

Hydrazoic acid (HN_3) is a member of a class of energetic molecules. Although its bond energy relative to formation of ground-state NH(X) and N_2 is very small (∼4000 cm^{-1}), it is fairly stable due to the fact that the dissociation of ground-state HN_3 to the lowest asymptote is spin-forbidden

$$HN_3\,(X^1A') \rightarrow N_2\,(X^1\Sigma_g^+) + NH\,(X^3\Sigma^-) \qquad (1)$$

Decomposition according to reaction 1 can occur by a spin−orbit-induced crossing between the singlet surface, which correlates asymptotically to N_2 ($X^1\Sigma_g^+$) + NH ($a^1\Delta$), and the lowest triplet surface. The crossing point can be considered as the "transition state" of the spin-forbidden reaction 1. The barrier height of 12 700 cm^{-1} was estimated by Kajimoto et al.[1] from thermal dissociation studies in a shock tube. High-resolution spectra for the predissociative N−H stretching overtone of HN_3 have yielded a considerably different activation energy (∼15 100 cm^{-1})[2,3] for reaction 1.

The spin-allowed process

$$HN_3\,(X^1A') \rightarrow N_2\,(X^1\Sigma_g^+) + NH\,(a^1\Delta) \qquad (2)$$

has been investigated by King and co-workers.[4,5] The NH ($a^1\Delta$) fragments were found to be translationally excited. This implies the existence of a barrier in the exit channel (∼1700 cm^{-1} with respect to the dissociation products). The relative enthalpy of the other spin-allowed product channel

$$HN_3\,(X^1A') \rightarrow N_3\,(X^2\Pi_g) + H\,(^2S) \qquad (3)$$

plays an important role in determining the relative branching ratios in the UV dissociation of HN_3, as well as controlling the exothermicity of the abstraction, reaction

$$H\,(^2S) + N_3\,(X^2\Pi_g) \rightarrow N_2\,(X^1\Sigma_g^+) + NH\,(X^3\Sigma^-) \qquad (4)$$

which has been studied in Dagdigian's laboratory.[6,7]

In many ways the HN_3 molecule is an ideal system for investigating the photodissociation process. Single-photon photodissociation experiments on HN_3 at 308,[8] 283,[9] 266,[8] and 248[10,11] nm show that the dominant product channel is

$$HN_3\,(X^1A') + h\nu \rightarrow HN_3\,(A^1A'') \rightarrow N_2\,(X^1\Sigma_g^+) + NH\,(a^1\Delta) \qquad (5)$$

Measurements of vibrational and rotational state distributions on both the NH and N_2 fragments[8−12] find large rotational excitation of the N_2 product but only modest internal excitation of the NH fragment. The distribution of the available energy among the various degrees of freedom of the fragments N_2 and HN, i.e., relative translation, rotation, vibration, and electronic excitation, has been analyzed in great detail for reaction 5. The UV photodissociation of HN_3 at 193 nm was investigated in detail in the bulk phase at 300 K. NH radicals in the $X^3\Sigma^-$, $a^1\Delta$, $b^l\Sigma^+$, $A^3\Pi$, and $c^1\Pi$ states were found to be formed simultaneously, but with very different quantum yields. The N_3 fragment and H atom as primary products of the HN_3 photodissociation at 248 and 193 nm were observed by Comes and co-workers[13]

$$HN_3\,(X^1A') + h\nu \rightarrow HN_3\,(A^1A'') \rightarrow N_3\,(X^2\Pi_g) + H\,(^2S) \qquad (6)$$

The photolysis of HN_3/DN_3 to give H/D and N_3 was further investigated at different photolysis wavelengths.[14] Nascent H/D atoms were characterized via Doppler and polarization spectroscopy using laser-induced fluorescence in the vacuum-ultraviolet region. The quantum yields have been found to be 0.04, 0.2, and 0.14 at 266, 248, and 193 nm, respectively. State-selected photodissociation of HN_3 has been studied by vibrationally exciting the molecule in the region of the second overtone of its H−N stretching motion and then photodissociating it using 532 nm light.[15] Measurement of the resulting NH fragment rotational state distribution reveals that photodissociation from initial nuclear configuration with an extended N−H bond leads to a substantially hotter rotational state distribution

† E-mail: fangwhgbnu.edu.cn.

10.1021/jp993386c CCC: $19.00
Published on Web 04/06/2000

than from nearly isoenergetic single-photon dissociation at 355 nm. Recently, the VUV photolysis of hydrazoic acid was reinvestigated by Stuhl and co-workers.[16] The fragment NH/ND ($c^1\Pi$) is formed with the same quantum yield below 147 nm, while the relative production yield of NH/ND ($A^3\Pi$) increases with decreasing wavelength. The near-ultraviolet photolysis of HN_3 has been investigated at a range of wavelengths, $\lambda \geq 240$ nm, using the technique of H Rydberg atom photofragment translational spectroscopy.[17] The deduced N_3 (X) product rotational energy disposal can be reproduced by an impulse model, which yields a refined measure of the H−N_3 bond strength, D_0(H−N_3) = 30 970 ± 50 cm^{-1}. The N_3 (X) product vibrational progressions observed at each photolysis wavelength "break off" at a low kinetic energy release. This is interpreted by invoking a barrier to dissociation via H−N bond fission on the A^1A'' state potential energy surface. Dissociation of HN_3 into HN and N_2 was used as a model for studying the specific phase correlations between reactive and nonreactive modes during the final few vibrations prior to reaction.[18]

In comparison, the HN_3 photodissociation has received less attention from a theoretical point of view. Alexander et al.[19,20] have carried out large-scale MCSCF and CI calculations, which mainly concentrated on the crossing between the ground-state singlet and the lowest triplet-state surfaces and on the barriers and dissociation energies for the spin-forbidden and spin-allowed decomposition of HN_3 in the ground state. Yarkony[21] has also performed MCSCF and CI calculations for these two states and has calculated the spin−orbit coupling matrix elements between them in the crossing region. The potential energy curves of the five lowest singlet and the five lowest triplet valence states of HN_3 along the interior N−N distance have been calculated by Meier and Staemmler[22] with *ab initio* CASSCF and valence CI methods. The angular dependence of the energy for the first excited singlet state was discussed. However, in their calculation the terminal N−N and N−H bond lengths are kept fixed at the ground-state equilibrium values, and the bond angles, N−N−N and N−N−H, are varied independently. The resulting potential energy profiles for dissociation of HN_3 to NH and N_2 are only qualitatively reliable. For the interpretation of the absorption spectrum, a series of quantum chemical *ab initio* calculations[16] at various levels of sophistication have been performed: SCF, valence CI with different active spaces, CASSCF, and multiconfiguration coupled electron-pair approach (MC-CEPA). All calculations were performed at the fixed equilibrium geometry of the planar ground state of HN_3. In the present paper, the potential energy surfaces governing HN_3 dissociation to HN + N_2 and H + N_3 in the ground (S_0), excited triplet (T_1), and singlet (S_1) states are fully optimized with the CASSCF method. The mechanism leading to different products is determined on the basis of the calculated potential energy surfaces and their crossing points. A comparison is made among the present and previous theoretical results and experimental findings.

Computational Details

The stationary-point structures on the ground and the first excited electronic states are optimized at the CASSCF[23] levels with the C_s symmetry constraint. The optimization was terminated when the maximum force and its RMS were less than 4.5×10^{-4} and 3.0×10^{-4} hartree/bohr, respectively. At the CASSCF converged geometry, the harmonic frequencies are calculated at the same level of theory with a cc-pVDZ basis set to confirm the resulting geometry to be the minimum or the first saddle point on the potential energy surfaces. Some stationary structures on the S_0 surface are also determined with the MP2(FC) energy gradient, where FC denotes the frozen 1s core of nitrogen atoms. The stationary structures are optimized with the cc-pVDZ and cc-pVTZ[24] basis sets. The intersection point between the S_0 and S_1 or T_1 surfaces is determined with the state-averaged CASSCF method with the cc-pVDZ basis set. Energies are calculated at the CASSCF-optimized structures with the multireference MP2 approach[25] (CASPT2) which was developed by Robb and co-workers. In calculation of barrier height and adiabatic excitation energy, a factor[26] of 0.85 is used to scale the calculated zero-point energies. All the calculations have been performed using the Gaussian 94 or G98W package of programs.[27]

To determine the height of the barrier in the ground state as well as the structure of the crossing point between the ground and the lowest triplet states, Alexander et al.[20] have used an active space with 16 valence electrons in 11 orbitals for the CASSCF calculations. Since the terminal N−N σ orbital is doubly occupied with a very low orbital energy, this orbital is excluded from the active space in the present CASSCF calculations. In addition, the initial test CASSCF calculations with 14 electrons in 10 orbitals for some geometries show that there are 3 orbitals with occupancies near 2, which are deleted from the molecular orbital space. Finally, an active space with eight electrons distributed in seven orbitals is used here, referred to as CAS(8,7). The energy of the separated fragments is determined by a supermolecule calculation, including both fragments at a large separation, with the same basis set and active space as for the calculation of the bound fragments.

In the limit that energy flows rapidly and randomly among all the vibrational degrees of freedom, the rate at which the molecule passes through the transition state from reactants to products may be calculated with the RRKM theory.[28] The rate coefficient for reaction when the molecule contains total energy E and has total angular momentum J is given by

$$k(E,J) = W(E,J)/h\rho(E,J)$$

where $\rho(E,J)$ is the density of states of the reactants as a function of E and J, h is Planck's constant, and $W(E,J)$ is the number of energy levels for vibration orthogonal to the reaction coordinate at the transition-state configuration with energy less than E. They can be, respectively, expressed as

$$W(E) = \sum_i^{\text{states}} H(E-E_i)$$

and

$$\rho(E) = \mathrm{d}W/\mathrm{d}E = \sum_i^{\text{states}} \delta(E-E_i)$$

where $H(E-E_i)$ and $\delta(E-E_i)$ are the Heaviside and delta functions, respectively. In practice the energy levels are obtained by assuming a rigid rotor-harmonic oscillator approximation:

$$\epsilon_{n,J,K} = W_{J,K} + \sum_i^s \hbar\omega_i(n_i + 1/2)$$

As pointed out by Miller,[28] the energy levels of most asymmetric rotors are reasonably well approximated by assuming an "almost symmetric top"; we invoke that approximation here, so that

$$W_{J,K} = (1/2)(A+B)[J(J+1) - K^2] + CK^2$$

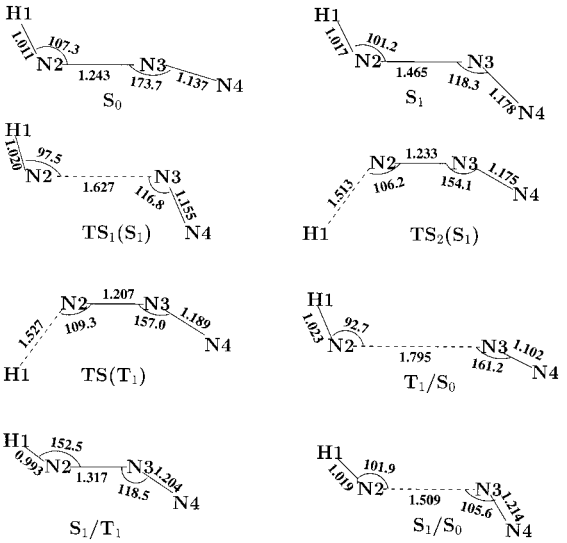

Figure 1. Schematic structures of the stationary and crossing points on the S_0, T_1, and S_1 surfaces of HN_3 (bond lengths in angstroms and bond angles in degrees).

A and *B* are chosen as the two most nearly equal rotation constants of the three *A*, *B*, and *C*.

Results and Discussion

Equilibrium Geometries of HN_3 in Its Ground and Excited States. Although several *ab initio* studies[16,19−22] of HN_3 have been performed, which always used the experimental structure, the equilibrium geometry of HN_3 in its ground electronic state (S_0) was not optimized at a more advanced level of theory. The equilibrium structure of HN_3 in S_0 is first optimized at the CAS-(8,7) and CAS(14,10) levels with the cc-pVDZ basis set. The resulting geometric parameters are close to the experimental values,[29] but the CAS(14,10) optimization does not give a better description of the equilibrium geometry than the CAS(8,7) calculation, as compared with the experimental structure. With increasing size of the basis set to cc-pVTZ, the optimized structure is still not improved with respect to the experimental geometry. The structure of HN_3 (S_0) is planar with a nearly linear N_3 moiety and the H−N bond strongly bent with respect to the N_3 backbone, as shown in Figure 1. It is of A′ symmetry. A natural orbital analysis of the total density based on the CAS-(8,7)/cc-pVDZ calculated wave functions shows that there are three doubly-occupied π molecular orbitals, numbered MO9, MO10, and MO11. These orbitals can be approximately represented as $\varphi(\mathrm{MO9}) = 0.68(2p_z(N_2)) + 0.56(2p_z(N_3)) + 0.05(2p_z(N_4))$, $\varphi(\mathrm{MO10}) = 0.15(2p_x(N_2)) - 0.67(2p_x(N_3)) - 0.64(2p_x(N_4))$, and $\varphi(\mathrm{MO11}) = 0.38(2p_z(N_2)) - 0.44(2p_z(N_3)) - 0.78(2p_z(N_4))$. This is consistent with the HN_3 molecular valence bond structure, H−N═N≡N. Finally, it should be mentioned that an attempt to optimize a *cis* minimum of HN_3 in S_0 does not converge, and instead leads to formation of the *trans*-HN_3 shown in Figure 1.

To our knowledge, no experimental or theoretical equilibrium geometry of HN_3 in its first excited electronic state (S_1) has been reported in the literature. This geometry is optimized here at the CAS(8,7) level of theory with the cc-pVDZ and cc-pVTZ basis sets. The obtained results with the two basis sets are close to each other. HN_3 (S_1) has a *trans* planar conformation with A″ symmetry, as shown in Figure 1 where the CAS(8,7)/cc-pVDZ parameters are also given. No *cis* minimum was found on the S_1 surface for HN_3. Unlike that in the ground electronic state, the N−N−N angle is close to 120° in S_1, and the interior and the terminal N−N bond lengths are increased by about 0.23 and 0.04 Å from S_0 to S_1, respectively. A natural orbital analysis shows that there are two singly-occupied π orbitals for the HN_3 molecule in S_1. One is a bonding π orbital like the MO11 in S_0; the other is an antibonding π^* orbital which is composed of p_x atomic orbitals of the three N atoms. One electron excitation from the π to π^* orbital makes the interior N−N π bond nearly broken and the terminal N−N π bond weakened, which is responsible for a significant increase of the interior N−N bond length and considerable change in the terminal N−N bond length from S_0 to S_1. From the viewpoint of valence bond theory, one electron excitation from S_0 to S_1 accompanies a rehybridization of the middle N atom from sp to sp^2, which results in a change in the N−N−N bond angle from 171.8° in S_0 to 118.3° in S_1.

The adiabatic excitation energy from S_0 to S_1 is 73.0 kcal/mol calculated with the CASPT2/cc-pVTZ approach on the CAS(8,7)/cc-pVTZ optimized structures. It becomes 71.9 kcal/mol with the scaled CAS(8,7)/cc-pVDZ zero-point energy correction. This may be compared with the experimental 0−0 excitation energy, but the 0−0 energy gap for HN_3 is not experimentally reported up to date. Recently, the single-photon UV photodissociation experiments[15] at 355 nm produce an NH fragment in the $^1\Delta$ electronic state. Compared with the corresponding vertical excitation energy of 80.5 kcal/mol (355 nm), one can expect that the calculated adiabatic excitation energy is reasonable. It seems that an energy-minimum point was found on the lowest triplet (T_1) surface by Meier and Staemmler.[22] Since the internal coordinates, except for the interior N−N distance, were frozen in their calculations, the minimum obtained in that study probably is not a real energy minimum. An attempt to optimize the equilibrium geometry of HN_3 in T_1 does not converge; instead a transition state for reaction 4 is found, which will be discussed below.

Spin-Forbidden and Spin-Allowed Decomposition of HN_3 (S_0). Reaction 1 is a spin-forbidden process, and one can expect that the minimum-energy crossing point (T_1/S_0) between the lowest singlet and triplet surfaces would play an important role in this process. The T_1/S_0 structure, as shown in Figure 1, is optimized with the state-averaged CASSCF energy gradient technique with the cc-pVDZ basis set. The structure of this crossing point was also determined by Alexander et al.[19,20] and Yarkony.[21] Since the terminal N−N and N−H distances were held to the equilibrium values in the isolated molecules in their calculations, the full CAS(8,7)/cc-pVDZ optimization performed here should provide a better description of the structure of the crossing point. The crossing point lies 40.6 kcal/mol (14208.8 cm^{-1}) in energy above the ground-state minimum, which provides an estimation of the barrier height of the nonadiabatic reaction 1. From thermal dissociation studies in a shock tube, the height of the barrier was deduced to be 12 700 cm^{-1} by Kajimoto et al.[1] However, high-resolution spectra[2,3] for the predissociative N−H stretching overtone of HN_3 have shown that when the overtone pumping frequency is increased to 15 100 cm^{-1}, the lifetime of HN_3 drops abruptly, which suggests that the activation energy of reaction 1 lies at about 43.1 kcal/mol. This value is close to the present calculated result. The previous theoretical calculations have estimated the activation energy of 39.5−48.3 kcal/mol.[19−21]

Reaction 1 is endothermic by 9.2−12.3 kcal/mol.[30] The endothermic character cannot be well described by the single-reference SCF calculations, as pointed out by Alexander and coworkers.[20] On the basis of their CASSCF+CI calculations and the previous experimental excitation energy, the bond

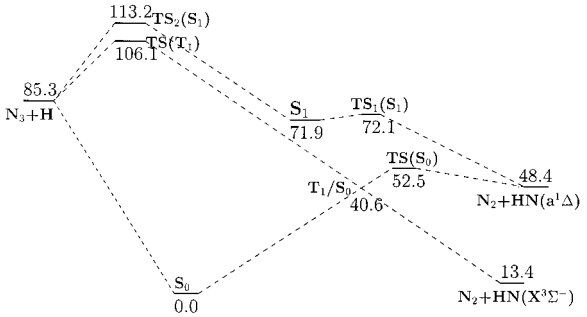

Figure 2. Schematic potential energy profiles of HN_3 (relative energies in kcal/mol with zero-pont energy correction).

dissociation energy (D_0) for the N_2 + NH ($X^3\Sigma^-$) asymptote was determined to be about 12 kcal/mol by them. The present CAS(8,7)/cc-pVTZ calculations give a dissociation energy of 6.7 kcal/mol. With the dynamic correlation considered at the CASPT2/cc-pVTZ level, it becomes 13.4 kcal/mol. The potential energy profile of the spin-forbidden decomposition is plotted in Figure 2.

The spin-allowed decomposition of HN_3 (S_0) to N_2 ($X^1\Sigma_g^+$) + NH ($a^1\Delta$) or N_3 ($X^2\Pi_g$) + H (^2S) has been studied by Alexander and co-workers[20] with the complete active space self-consistent field and multireference configuration interaction (CASSCF+MRCI) method and large basis sets. The resulting dissociation energies (D_0) of reactions 2 and 3 were 48.1 and 87.8 kcal/mol, respectively. The present CASPT2/cc-pVTZ calculations give dissociation energies of 48.4 for reaction 2 and 85.3 kcal/mol for reaction 3. Compared with the experimental estimations of 45.6−48.6 kcal/mol for reaction 2 and 86.8−96.9 kcal/mol for reaction 3,[2−5,17] both the present and the previous theoretical values are in excellent agreement with the experimental findings. No energy barrier above the endothermicity is found for reaction 3; however, a small barrier exists in the exit channel (reaction 2). The height of the barrier is estimated to be 4.1 kcal/mol.[20] The potential energy profiles of reactions 2 and 3 are summarized in Figure 2. The results from the present calculations are consistent with the previous theoretical and experimental findings where available, which gives us a reason to expect that the dissociation of HN_3 on the excited electronic states can be well described by the CAS(8,7) calculation.

Decomposition of HN_3 on the Excited Electronic States. Hydrazoic acid in its ground state is stable, due to the existence of the conjugation π system and the fact that the decomposition to the asymptote N_2 + NH ($X^3\Sigma^-$) is spin-forbidden. However, when the molecule is excited to the S_1 state, the interior N−N π bond is nearly broken and the direct dissociation, pathway 5, is spin-allowed. This gives us a hint that the dissociation of HN_3 in S_1 is much easier than that in S_0. A transition state [TS_1 (S_1)] is found on pathway 5 at the CAS(8,7)/cc-pVDZ and CAS-(8,7)/cc- pVTZ levels of theory. Figure 1 shows the CAS(8,7)/cc-pVDZ-optimized $TS_1(S_1)$ structure. Relative to the S_1 minimum of HN_3, the CAS(8,7)/cc-pVDZ and CAS(8,7)/cc-pVTZ calculations provide the same barrier height of 1.1 kcal/mol (385 cm^{-1}). It becomes 0.2 kcal/mol ($\sim$70 cm^{-1}) with the scaled CAS(8,7)/cc-pVDZ zero-point energy correction. The modest modulation on the absorption spectrum[31,32] of HN_3, $S_1 \leftarrow S_0$, is a hint for an insignificant potential barrier of reaction 5. No strong potential barrier was found along the interior N−N separation in the photofragmentation dynamics[11] of hydrazoic acid from its lowest excited singlet state. A direct dissociation mechanism of $HN_3(A^1A'')$ was deduced by Chu et al.[9] and also by Hawley and co-workers.[12] In a set of recent experiments[33,34] on photodissociation of the isoelectronic HNCO molecule, a barrier in the exit channel of the HNCO (S_1) to NH ($a^1\Delta$) + CO ($X^1\Sigma^+$) was estimated in the range of 500 cm^{-1}. High-level calculations by Schinke and co-workers[35] have also predicted a barrier height of about 550 cm^{-1} (without zero-point energy correction). The HN_3 molecule with three electronegative N atoms is inherently less stable than the HNCO molecule with a more electropositive element between the electronegative ones. Therefore, the barrier of the HN_3 dissociation is expected to be lower than that of the HNCO dissociation.

The interior N−N distance is increased by 0.162 Å from the reactant of HN_3 (S_1) to the transition state of TS_1 (S_1), while the other bond parameters are only slightly varied in TS_1 (S_1) with respect to those in HN_3 (S_1). As anticipated by Hammond's postulate,[36] the exothermic reaction has a transition-state geometry close to that of the the reactant. The structures of HN_3 (S_1) and TS_1 (S_1), as in Figure 1, are both *trans* planar, which have been confirmed to be minimum and saddle points on the S_1 surface, respectively. From the observed $\mathbf{v}-\mathbf{J}$ and $\boldsymbol{\mu}-\mathbf{v}-\mathbf{J}$ vector correlations,[8,9,37] however, the dissociation of HN_3 (S_1) into NH ($a^1\Delta$) and N_2 ($X^1\Sigma^+_g$) is predicted to proceed via a nonplanar motion of the NH rotor. The interior N−N bond length is about 1.6 Å in TS_1 (S_1); the rotation of the NH moiety is not completely free. Thus, TS_1 (S_1) maintains the planar symmetry of the reactant. After the system passes through the saddle point on the S_1 surface, the interior N−N separation is larger. In this case, it is easier for the NH moiety to distort from the initial molecular plane. Therefore, the optimized planar structures of HN_3 (S_1) and TS_1 (S_1) are not inconsistent with the vector correlation experiments mentioned above.

On the basis of the optimized structures of HN_3 (S_1) and TS_1 (S_1), the available energy distribution in the nascent fragments can be roughly estimated with a simple impulse dissociation model.[38] More than half of the available energy is changed into translational energy of the fragments. The rest is mainly dumped into rational states of N_2 and vibrational states of NH. Less than 1% of the available energy is distributed in vibrational states of N_2 and rotational states of NH. These clearly show that the nascent N_2 is in its vibrational ground state and rotational excited states, whereas the nascent NH is in its vibrational excited states. All of these are consistent with the experimental findings.

In addition to dissociation to HN and N_2, the HN_3 molecules in S_1 can also decompose into N_3 ($X^2\Pi_g$) + H (^2S), namely, pathway 6. A transition state on this pathway [TS_2 (S_1)] is found, as shown in Figure 1. Again, optimizations with the cc-pVDZ and cc-pVTZ basis sets provide nearly the same structural parameters for TS_2 (S_1), in which the H−N bond is almost broken and the N−N−N moiety is close to the N_3 radical in structure. Analysis of the N_3 (X) product vibrational progressions[17] shows that a barrier exists on the S_1 pathway, $HN_3 \rightarrow H + N_3$. The observed energy disposals and the deduced impact parameters predict that the departing H atom is directed at $\sim$90° to the near linear N_3 chain. The optimized structure of TS_2 (S_1) in Figure 1 is in agreement with this experimental prediction. It should be pointed out that an attempt to search for a *trans* transition state does not converge, and instead leads to formation of TS_2 (S_1) that has a *cis* conformation. The optimization process of TS_2 (S_1) shows that departure of the hydrogen atom accompanies an isomerization from the *trans* to *cis* conformation. In fact, there is little difference between the *trans* and *cis* conformations, when the N−H separation is large and the N−N−N configuration is close to being linear. The dissociation of HN_3 (S_1) into N_3 ($X^2\Pi_g$) and H (^2S) is endothermic by 12.4

kcal/mol with a barrier of 39.7 kcal/mol at the CAS(8,7)/cc-pVTZ level, including the scaled CAS(8,7)/cc-pVDZ zero-point energy correction. On the CAS(8,7)/cc-pVTZ-optimized stationary structures, the endothermic character and barrier height of the reaction are further calculated to be 13.4 and 41.3 kcal/mol, respectively, with the multireference MP2 approach. The potential energy profile of the reaction is depicted in Figure 2.

Single-photon photodissociation experiments on HN_3 at 355, 308, 283, and 266 nm find that the products are exclusively N_2 ($X^1\Sigma_g^+$) + NH ($a^1\Delta$). The corresponding vertical excitation energy is in the range from 80.5 to 107.4 kcal/mol. Upon inspection of Figure 2, one can see that the TS_1 (S_1) and TS_2 (S_1) lie 72.1 and 113.2 kcal/mol in energy above the HN_3 (X^1A') zero-point vibrational level. It is obvious that channel 5 is energetically accessible, but channel 6 not accessible in energy to photodissociation at 355−266 nm. The N_3 ($X^2\Pi_g$) and H (^2S) were found as minor products at 248 nm photodissociation.[10,11] In this case the excitation energy of 115.3 kcal/mol is a little higher than the barrier energy of channel 6; thus, reaction 6 can occur, but with lower yield compared with reaction 5. The energies calculated above are in excellent agreement with the photodissociation experiments of HN_3.

Mechanism of HN_3 Photodissociation. After photoexcitation in a wavelength range from 355 to 248 nm, the HN_3 molecules populate in the first excited electronic state (S_1). From this state, in addition to radiative decay, there are three possible pathways for HN_3 to deactivate. The first pathway involves the dissociation to N_2 ($X^1\Sigma_g^+$) + NH ($a^1\Delta$) or N_3 ($X^2\Pi_g$) and H (^2S) on the S_1 surface. Since some excess energy is dumped into vibrational modes, the reactions cannot be viewed correctly as rolling along the minimum-energy path of the potential energy surface with locally zero kinetic energy. The RRKM theory can be used to estimate the rates of these processes. On the basis of the calculated vibrational frequencies, rotational constants, and energies, the RRKM rate coefficients of reactions 5 and 6 as a function of total energy and total angular momentum are computed. When the molecule contains the total energy of 43 kcal/mol [relative to the zero-point vibrational level of HN_3 (S_1)], and has total angular momentum $J = 20$, the rate coefficient of the HN_3 (S_1) dissociation to N_3 ($X^2\Pi_g$) and H (^2S) is 3.72×10^8 s^{-1} which is negligibly small in comparison with the rate coefficient of 2.17×10^{13} s^{-1} for reaction 5. If the IC rate from S_1 to S_0 is in the higher limit, which is discussed below, the RRKM rate coefficients of both reactions 5 and 6 will be decreased, as the state density of the ground-state reactant makes an important contribution to the RRKM-calculated rate coefficient. In addition, the rate coefficient of reaction 5 has approached the applicability limit of the RRKM theory, which assumes the species are vibrationally equilibrated, as the time scale of vibrational relaxation, in general, is in the range of a picosecond or a subpicosecond. Although there is an error in the calculated rate coefficients, we can say that channel 6 cannot compete with channel 5 at 248 nm and longer wavelength photodissociation of HN_3.

The second possible pathway is intersystem crossing (ISC) to the lowest triplet state (T_1) and followed by dissociation. An intersection point between the S_1 and T_1 surfaces (S_1/T_1) is found with the state-averaged CAS(8,7)/cc-pVDZ method. Its structure is shown in Figure 1. The S_1/T_1 point lies 36.1 kcal/mol in energy above the S_1 minimum, therefore much higher than the barrier height of the direct dissociation reaction 5. A qualitative analysis by Turro[39] predicted the ISC from S_1 ($^1\pi\pi^*$) to T_1 ($^3\pi\pi^*$) to be inefficient, since there is no first-order spin−orbit coupling between the two states. On the other hand, if the coupling between S_1 and T_1 in HN_3 is strong, the ground-state products of N_2 ($X^1\Sigma_g^+$) and NH ($X^3\Sigma^-$) should be experimentally observed, as the T_1 surface is repulsive with respect to the interior N−N separation. However, N_2 ($X^1\Sigma_g^+$) and NH ($a^1\Delta$) were exclusively observed as the primary products in the single-photon dissociation of HN_3 at the 355−266 nm. Recently, Reisler and co-workers[40] have investigated fragment recoil anisotropies on the photoinitiated decomposition of HNCO. They concluded that direct $S_1 \rightarrow T_1$ coupling is much weaker than $S_1 \rightarrow S_0$ internal conversion (IC). All of these give us a reason to expect that the ISC from S_1 to T_1 takes place with very low efficiency and is negligible with respect to the direct dissociation on S_1.

The third pathway involves IC to the ground state. The intersection point between the S_1 and S_0 surfaces (S_1/S_0) plays an important role in the IC process. The S_1/S_0 point is optimized with the state-averaged CAS(8,7)/cc-pVDZ approach. The resulting structure is depicted in Figure 1 along with its geometric parameters. Obviously, the S_1/S_0 point is closer to the S_1 minimum in structure than to the S_0 minimum. It should be pointed out that the S_1/S_0 point is not on the dissociation pathway of HN_3 (S_1) to N_2 ($X^1\Sigma_g^+$) and NH ($a^1\Delta$), although the interior N−N separation in the S_1/S_0 structure lies between the corresponding values in the S_1 and TS_1 (S_1) structures. This is because the terminal N−N separation in the S_1/S_0 structure is longer than that in the S_1, TS_1 (S_1), or N_2 structure. The S_1/S_0 point is 29.0 kcal/mol lower in energy than the S_1/T_1 point, but 6.9 kcal/mol higher than the barrier height of the direct dissociation reaction 5. The $S_1 \rightarrow S_0$ IC occurs more easily than the $S_1 \rightarrow T_1$ ISC, but the dissociation reaction 5 still prevails, due to a very small barrier on the pathway. The rate of the IC from S_1 to S_0 in ketene (H_2CCO)[41] was experimentally estimated to be in the range of 2.5×10^9 to 4.0×10^{13} s^{-1}. Since H_2CCO is an isoelectronic molecule of HN_3, and their electronic and geometric structures are similar to each other, one can assume that the IC rate from S_1 to S_0 for HN_3 is in a similar range. The lower limit of the IC rate is negligibly small, as compared with the rate of the direct dissociation of HN_3 (S_1) to N_2 ($X^1\Sigma_g^+$) and NH ($a^1\Delta$). In this case, the HN_3 molecule is excited to S_1 and followed by the direct dissociation, which is the most probable mechanism of the HN_3 photodissociation at a wavelength range from 355 to 248 nm.

If the IC rate lies in the higher limit of 4.0×10^{13} s^{-1}, the direct dissociation on S_1 and the IC to the ground electronic state are a pair of competitive pathways. The HN_3 molecules which return to the ground state are left with sufficient internal energy to undergo the spin-conserved dissociation to N_2 ($X^1\Sigma_g^+$) + NH ($a^1\Delta$) and the spin-forbidden dissociation to N_2 ($X^1\Sigma_g^+$) + NH ($X^3\Sigma^-$), but the spin-allowed dissociation to N_3 ($X^2\Pi_g$) and H (^2S) cannot compete with the above two ground-state processes, due to its high endothermic character. Time-domain measurements of dissociation rate in S_0 have been reported for different vibrational levels.[3] It has been found that the rate of the spin-forbidden dissociation is overestimated by a factor of about 10^4 if the dissociation is treated as a spin-allowed process. That is, the $S_0 \rightarrow T_1$ ISC occurs with probability close to a value of 10^{-4}. So, the spin-forbidden dissociation reaction 1 cannot compete with the spin-allowed process 2, although the T_1/S_0 intersection point is a little lower in energy than TS_1 (S_0), as seen in Figure 2. The HN_3 molecules populated in S_1 relax back to the ground electronic state; thus, the dominant product channel is still N_2 ($X^1\Sigma_g^+$) and NH ($a^1\Delta$), due to a very small $S_0 \rightarrow T_1$ probability which decreases the rate of the spin-forbidden dissociation reaction 1. This provides a good explana-

tion of the experimental fact that NH ($a^1\Delta$) is formed with a quantum yield of 0.4, while the NH ($X^3\Sigma^-$) yield is less than 0.002 in the UV photolysis[10] of HN_3 at 193 nm.

As shown in Figure 2, when $N_3(X^2\Pi_g)$ and H (^2S) approach each other, there exist three spin-conserved pathways leading to HN_3 (S_0), HN_3 (S_1), and N_2 ($X^1\Sigma_g^+$) + NH ($X^3\Sigma^-$). The first two have been discussed before. The last one is reaction 4. A transition state [TS (T_1)] shown in Figure 1 is found on this triplet pathway. The optimized TS (T_1) is similar in structure to that of reaction 6. The barrier height of reaction 4 is 20.8 kcal/mol, which is 7.1 kcal/mol lower in energy than that of the reverse process of reaction 6.

Summary

In the present work, photodissociation of HN_3 at long wavelength (355−248 nm) is investigated with the complete active space SCF molecular orbital method. The mechanism leading to different products is determined on the basis of the optimized ground- and excited-state potential energy surfaces of dissociation and their crossing points. After the HN_3 molecules are excited to the S_1 state, the most probable pathway is direct dissociation of HN_3 (S_1) into N_2 ($X^1\Sigma_g^+$) and NH ($a^1\Delta$), due to a very small barrier on the pathway. A high barrier exists on the S_1 pathway to N_3 ($X^2\Pi_g$) + H (^2S), which is nearly inaccessible in energy at the long-wavelength region. Thus, the decomposition of HN_3 (S_1) to N_3 ($X^2\Pi_g$) + H (^2S) cannot compete with the direct dissociation to N_2 ($X^1\Sigma_g^+$) and NH ($a^1\Delta$). If the IC rate constant lies in the estimated higher limit, the $S_1 \rightarrow S_0$ IC is in competition with the direct dissociation. The HN_3 molecules in S_1 which return to the ground electronic state are left with sufficient internal energy to overcome the barrier of the spin-allowed dissociation to N_2 ($X^1\Sigma_g^+$) + NH ($a^1\Delta$) or the barrier of the spin-forbidden pathway to N_2 ($X^1\Sigma_g^+$) + NH ($X_3\Sigma^-$). A very small $S_0 \rightarrow T_1$ probability reduces the rate coefficient of the spin-forbidden dissociation by a factor of about 10^4. Therefore, the dominant product channel is still N_2 ($X^1\Sigma_g^+$) + NH ($a^1\Delta$), as in S_1. The present calculations provide a good elucidation that the NH fragments are exclusively in the $a^1\Delta$ state in the UV photodissociation of HN_3 at a wavelength range from 355 to 248 nm. The triplet potential energy surface is repulsive with respect to the interior N−N separation. When N_3 ($X^2\Pi_g$) and H (^2S) approach each other along the triplet pathway, reaction 4 can occur, forming the ground-state products of N_2 ($X^1\Sigma_g^+$) + NH ($X^3\Sigma^-$), but it is more efficient for N_3 ($X^2\Pi_g$) and H (^2S) to combine, forming the ground-state reactant of HN_3.

Acknowledgment. This work was supported by the National Natural Science Foundation of China (Grant No. 29673007). I am grateful to the Alexander von Humboldt Foundation for donation of an IBM/RS6000 workstation.

References and Notes

(1) Kajimoto, O.; Yamamoto, T.; Fueno, T. *J. Phys. Chem*. **1979**, *83*, 429.
(2) Foy, B. R.; Casassa, M. P.; Stephenson, J. C.; King, D. S. *J. Chem. Phys*. **1989**, *90*, 7037.
(3) Foy, B. R.; Casassa, M. P.; Stephenson, J. C.; King, D. S. *J. Chem. Phys*. **1990**, *92*, 2782.
(4) Stephenson, J. C.; Casassa, M. P.; King, D. S. *J. Chem. Phys*. **1988**, *89*, 1378.
(5) Casassa, M. P.; Foy, B. R.; Stephenson, J. C.; King, D. S. *J. Chem. Phys*. **1991**, *94*, 250.
(6) Chen, J.; Quinones, E.; Dagdigian, P. J. *J. Chem. Phys*. **1989**, *90*, 7603.
(7) Sauder, D. G.; Patel-Misra, D.; Dagdigian, P. J. *J. Chem. Phys*. **1989**, *91*, 5316.
(8) Gericke, K.-H.; Theinl, R.; Comes, F. J. *Chem. Phys. Lett*. **1989**, *164*, 605. Gericke, K.-H.; Theinl, R.; Comes, F. J. *J. Chem. Phys*. **1990**, *92*, 6548.
(9) Chu, J. J.; Marcus, P.; Dagdigian, P. J. *J. Chem. Phys*. **1990**, *93*, 257.
(10) Rohrer, F.; Stuhl, F. *J. Chem. Phys*. **1988**, *88*, 4788.
(11) Gericke, K.-H.; Haas, T.; Lock, M.; Theinl, R.; Comes, F. J. *J. Phys. Chem*. **1991**, *95*, 6104.
(12) Hawley, M.; Baronavski, F.; Nelson, H. H. *J. Chem. Phys*. **1993**, *99*, 2638.
(13) Gericke, K.-H.; Haas, T.; Lock, M.; Comes, F. J. *Chem. Phys. Lett*. **1991**, *186*, 427. Haas, T.; Gericke, K.-H.; Maul, C.; Comes, F. J. *Chem. Phys. Lett*. **1993**, *202*, 108.
(14) Lock, M.; Gericke, K.-H.; Comes, F. J. *Chem. Phys*. **1996**, *213*, 385.
(15) Barnes, R. J.; Gross, A.; Lock, M.; Sinha, A. *J. Phys. Chem. A* **1997**, *101*, 6133−6137.
(16) Schoennenbeck, G.; Biehl, H.; Stuhl, F.; Meier, U.; Staemmler, V. *J. Chem. Phys*. **1998**, *109*, 2210.
(17) Cook, P. A.; Langford, S. R.; Ashfold, M. N. R. *Phys. Chem. Chem. Phys*. **1999**, *1*, 45.
(18) Wright, K. R.; Hutchinson, J. S. *Phys. Chem. Chem. Phys*. **1999**, *1*, 1299.
(19) Alexander, M. H.; Werner, H.-J.; Dagdigian, P. J. *J. Chem. Phys*. **1988**, *89*, 1388.
(20) Alexander, M. H.; Werner, H.-J.; Hemmer, T.; Knowles, P. J. *J. Chem. Phys*. **1990**, *93*, 3307.
(21) Yarkony, D. R. *J. Chem. Phys*. **1990**, *92*, 320.
(22) Meier, U.; Staemmler, V. *J. Phys. Chem*. **1991**, *95*, 6111.
(23) Yamomoto, N.; Vreven, T.; Robb, M. A.; Frisch, M. J.; Schlegel, J. B. *Chem. Phys. Lett*. **1996**, *250*, 373.
(24) Dunning, T. H., Jr. *J. Chem. Phys*. **1989**, *90*, 1007.
(25) McDouall, J. J.; Peasley, K.; Robb, M. A. *Chem. Phys. Lett*. **1988**, *148*, 183.
(26) Scott, A. P.; Radom, L. *J. Phys. Chem*. **1996**, *100*, 16502.
(27) Gaussian 98 (Revision A.3): Frisch, M. J.; Trucks, G. W.; Schlegel, H. B.; Scuseria, G. E.; Robb, M. A.; Cheeseman, J. R.; Zakrzewski, V. G.; Montgomery, J. A.; Stratmann, R. E.; Burant, J. C.; Dapprich, S.; Millam, J. M.; Daniels, A. D.; Kudin, K. N.; Strain, M. C.; Farkas, O.; Tomasi, J.; Barone, V.; Cossi, M.; Cammi, R.; Mennucci, B.; Promelli, C.; Adamo, C.; Clifford, S.; Ochterski, J.; Petersson, G. A.; Ayala, P. Y.; Cui, Q.; Morokuma, K.; Malick, D. K.; Rabuck, A. D.; Raghavachari, K.; Foresman, J. B.; Cioslowski, J.; Ortiz, J. V.; Stefanov, B. B.; Liu, G.; Liashenko, A.; Piskorz, P.; Komaromi, I.; Gomperts, R.; Martin, R. L.; Fox, D. J.; Keith, T.; Al-Laham, M. A.; Peng, C. Y.; Nanayakkara, A.; Gonzalez, C.; Challacombe, M.; Gill, P. M. W.; Johnson, B. G.; Chen, W.; Wong, M. W.; Andres, J. L.; Head-Gordon, M.; Replogle, E. S.; Pople, J. A., Gaussian, Inc.: Pittsburgh, PA, 1998.
(28) Eyring, H; Lin, S. H.; Lin, S. M. *Basic Chemical Kinetics*; Wiley: New York, 1980. Miller, W. H. *J Am. Chem. Soc*. **1979**, *101*, 6810.
(29) Winnewisser, B. P. *J. Mol. Spectrosc*. **1980**, *82*, 220.
(30) Okabe, H. *Photochemistry of Small Molecules*; Wiley: New York, 1978.
(31) Okabe, H. *J. Chem. Phys*. **1968**, *49*, 2726.
(32) McDonald, J. R.; Rabalis, J. W.; McGlynn, S. P. *J. Chem. Phys*. **1970**, *52*, 1332.
(33) Droz-Georget, T.; Zyrianov, M.; Reisler, H.; Chandler, D. W. *Chem. Phys. Lett*. **1997**, *276*, 316.
(34) Brown, S. S.; Berghout, H. L.; Crim, F. F. *J. Chem. Phys*. **1996**, *105*, 8103.
(35) Klossika, J.-J.; Floethmann, H.; Beck, B.; Schinke, R.; Yamashita, K. *Chem. Phys. Lett*. **1997**, *176*, 325.
(36) Hammond, G. S. *J. Am. Chem. Soc*. **1955**, *77*, 334.
(37) Barnes, R. J.; Sinha, A.; Dagdigian, P. J.; Lambert, H. M. *J. Chem. Phys*. **1999**, *111*, 151.
(38) Tuck, A. F. *J. Chem. Soc., Faraday Trans. 2* **1977**, *73*, 689.
(39) Turro, N. J. *Modern Molecular Photochemistry*; Benjamin/Cummings Publishing Co., Inc.: Menlo Park, CA, 1978; pp 165−170.
(40) Zyrianov, M.; Droz-Georget, Th.; Reisler, H. *J. Chem. Phys*. **1999**, *110*, 2059.
(41) Chen, I-C.; Moore, C. B. *J. Phys. Chem*. **1990**, *94*, 263.